Received: 17 October 2018 | Revised: 3 December 2018 | Accepted: 4 December 2018

DOI: 10.1111/jace.16262

ORIGINAL ARTICLE

Journal of the American Ceramic Society

Determination of ceramic flaw populations from component strengths

Robert F. Cook[1] | **Frank W. DelRio**[2]

[1]Materials Measurement Science Division, National Institute of Standards and Technology, Gaithersburg, Maryland

[2]Applied Chemicals and Materials Division, National Institute of Standards and Technology, Boulder, Colorado

Correspondence
Robert F. Cook, Materials Measurement Science Division, National Institute of Standards and Technology, Gaithersburg, MD.
Email: robert.cook@nist.gov

Abstract

A procedure is outlined for determining the population of flaws in manufactured ceramics from strength measurements of sampled components. The broad applicability of the procedure is demonstrated in a quantitative manner, using strength measurements from a range of ceramic materials (eg, glass, glass-ceramic, single crystal, and polycrystal) with different flaw types (eg, bulk, surface, and edge). The deconvoluted flaw populations are mostly dominated by small flaws with extended large flaw tails and are all in domains of tens of micrometers. The procedure greatly extends the useful information to be gained by ceramics manufacturers and designers from strength distribution measurements and emphasizes the importance of identifying strength-limiting characteristics within a flaw population.

KEYWORDS

distribution, flaw, manufacturing, probability, strength

1 | INTRODUCTION

Manufacturing processes for load-bearing components or materials are optimized to fabricate components that can bear the greatest load or materials that exhibit the greatest strength, subject to the constraints of cost, weight, timeliness, environmental impact, etc.[1] In particular, manufacturing processes for many structural ceramics optimize brittle fracture strength by minimizing the number and magnitude of strength-limiting flaws, usually cracks, in the ceramic. In addition to optimizing strength, information regarding ceramic flaw populations is also critical: to optimize *yield* in manufacturing, if flaws are defects that limit the strength of manufactured components; to estimate *reliability* in use, if flaws become defects that limit the lifetime of operational components; and, to extrapolate *design* parameters, if flaws limit size or shape of innovative components. A common method of assessing the population of flaws in a manufactured ceramic material is to measure the distribution of fracture strengths in a group of components sampled from the material. Usually, the group consists of specially formed components (eg, bend bars) comprising a small volume of test material sampled (eg, by sawing) from the larger entirety of manufactured material volume. Manufacturers usually seek to minimize cost and maximize timeliness by minimizing the sampled volume relative to the manufactured material volume. Hence, there is a commercial driving force to obtain as much information as possible regarding the population of flaws imbedded in an entire volume of manufactured ceramic from the distributions of strengths characterizing the much smaller volumes of sampled test components.

A recent work[2] considered in some detail the relationship between the flaw population in a volume of manufactured material and the strength distribution exhibited by a sampled group of test components. The relationship was considered in two ways: (a) a "forward" direction, in which a known flaw population was used to predict resulting strength distributions based on the volume and number of the test components; and, (b) a "backward" direction, in which an empirical component strength distribution was used to infer the underlying material flaw population. The sensitivity of both forward predictions and backward inferences to the number of measurements and the ratio of (sample volume)/(manufactured material volume) were highlighted, especially the influences of these factors in fully characterizing flaw populations from strength distribution parameters. Attention

was focused on deconvoluting strength distributions of ultra-small components formed by chemical etching or growth processes (ie, microelectromechanical systems [MEMS] devices and nanowires) to infer nano-scale flaw population characteristics. Strengths of a few gigapascals up to a few tens of gigapascals were used to examine cracks a few tens of nanometers in size down to about a nanometer.

Here, a similar methodology is applied to deconvolute strength distributions of a wide range of ceramic components and determine *micro-scale* flaw populations. Mechanical (eg, polishing, sawing, sharp contact) and thermal (eg, sintering, heat treatment) processes often encountered in ceramic manufacturing are considered. As noted in a review of MEMS strengths,[3] different surface treatments (eg, chemical and mechanical) used to manufacture components of different scales usually generate brittle fracture strength-controlling surface flaws of systematically different magnitudes. For example, mechanically formed components are typically larger than chemically formed components and contain larger surface flaws. Similarly, thermally formed components are large and contain large strength-controlling bulk flaws. Such correlations are well known in engineering design, in which manufactured component tolerances and surface roughness scale with component size.[1] Hence, the ceramic components to be examined here exhibit micro-scale flaw population characteristics. Strengths of several hundred megapascals are examined, reflecting underlying flaws tens of micrometers in size.

The work begins by developing the analysis required to deconvolute flaw populations from strength distributions, extending that used previously[2] to include ceramics-related considerations; a similar analysis was used to connect flaw populations and component lifetimes in a reliability context.[4] The analysis is followed by a description of the ceramic materials and systems to be studied, nine in all divided into four sets: cordierite, alumina, and silicon components containing dominant polishing or sawing flaws; glass, spodumene, and cordierite components containing dominant sharp indentation contacts; sintered silicon nitride components containing dominant pores; and, heat treated fused and tabular refractory alumina grains containing dominant voids. To optimize statistical assessment, each group of materials consists of about 100 components. The results are then presented as strength distributions and the conjugate flaw populations. The discussion emphasizes the applicability of the outlined procedure in manufacturing.

2 | ANALYTICAL METHODS

The analysis is divided into two sections. In the first section, an overall probabilistic framework is developed by consideration of forward prediction, from an assumed large population of flaws to strength distributions of sampled groups of components. In the second section, the framework is used in the reverse direction to use an experimentally measured group of strengths to deconvolute an underlying flaw population. A flexible smoothing function, required to describe measured strengths in implementation of the deconvolution procedure, is introduced in the second section, along with different strength-flaw size relationships required for the different flaw types in the four materials sets mentioned above.

2.1 | Strength distribution prediction

Analysis begins by considering a manufacturing process that generates a ceramic, total volume Ω, containing a large population of brittle fracture strength-controlling features, Figure 1A. The features have an average density (number/volume) of λ. Such a density pertains to cases of strength-limiting features in the *bulk* of a ceramic (eg, pores in silicon nitride or internal voids in refractory alumina, see below). In many brittle ceramics strength-limiting features occur preferentially on the damaged *surface* of a material (eg, polishing scratches on cordierite or sharp contact cracks on glass, see below) and it is useful to define a characteristic dimension h that is the surface depth of the damage. Ω/h is then interpreted as the area of the strength-limiting surface, Figure 1A and the product (λh) gives the areal density (number/area) of strength-limiting surface features. In other cases, strength limiting features occur along a damaged material *edge* (eg, silicon dicing damage or alumina sawing damage, see below) and it is useful to recognize h^2 as an area that is the characteristic internal extent of edge damage. The product (λh^2) gives the lineal density (number/length) of strength-limiting edge features. The reciprocals of the densities are somewhat more intuitive and areal density is used here in examples. The reciprocal of (λh) defines the area $\Delta A = 1/(\lambda h)$. ΔA is chosen to be sufficiently small (or λh sufficiently large) such that each area ΔA contains exactly one feature arising from the manufacturing process and ΔA thus defines a fundamental element of area, Figure 1A,B. A magnitude of the features relevant to strength varies from feature to feature. The primary intention and simplest interpretation is that the feature magnitude is a physical length dimension, c, representing a crack length that determines the local strength of the material. c is thus referred to as a "flaw size." (An obvious dimensional limitation in this case is that, on average, $c \leq \Delta A^{1/2}$). Fundamental elements of volume and length are analogously defined.[2] Other flaw size magnitudes, including dimensionless values, can also be used. For simplicity, ΔA and c are used here, but, with important noted exceptions, the following analysis is general.

The population of elements, $\Omega\lambda$, is considered sufficiently large that the flaw sizes may be treated as a continuum and thus there exists a continuous probability density function (pdf), $f(c)$, describing the flaw sizes over the domain $c_{\min} \leq c \leq c_{\max}$. $f(c)$ can be considered as the fundamental property of the population and $c_{\min}$ and $c_{\max}$ are the minimum and maximum flaw sizes, respectively. Integration of the pdf gives the cumulative distribution function (cdf), $F(c)$,[5]

$$F(c) = \int_0^c f(c')\mathrm{d}c'. \tag{1}$$

$F(c)$ gives the proportion of the population of elements with flaw sizes smaller than c and is thus the probability that an element selected at random from the population will have a flaw size smaller than c. Normalization of the pdf requires

$$\int_{c_{\min}}^{c_{\max}} f(c')\mathrm{d}c' = 1 \tag{2}$$

and, thus, $F(c)$ increases from 0 to 1 over the domain $c_{\min} \leq c \leq c_{\max}$. Equation (1) may be expressed as

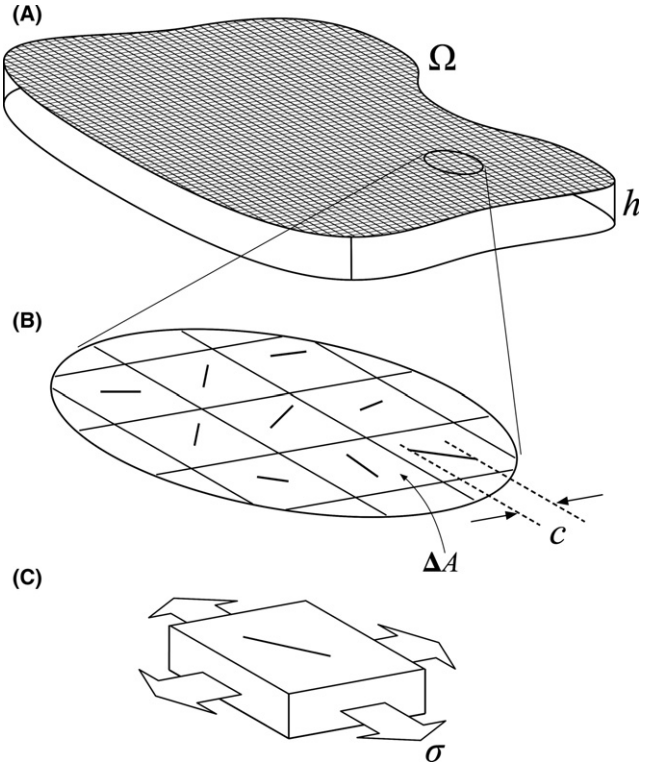

FIGURE 1 Schematic diagrams of a volume of manufactured material with strength controlled by surface flaws. A, The total volume, Ω, indicating surface damage layer h and division into a population of elemental areas. B, Enlargement showing elemental areas ΔA containing surface flaws of size c. C, Measurement of strength σ of an elemental area

$$f(c) = \frac{\mathrm{d}F(c)}{\mathrm{d}c} \tag{3}$$

enabling $f(c)$ to be determined if $F(c)$ is known. It is the experimental estimation of $f(c)$ that is a major focus of this work.

The pdf and cdf functions given above, $f(c)$ and $F(c)$, describe the population of flaw sizes. To make connection with the distribution of component strengths, a relationship between element strength and flaw size is required. As an example, for an element containing flaw size c the strength σ, Figure 1C, can be expressed by the Griffith relation[6]

$$\sigma = Bc^{-1/2}, \tag{4}$$

where B is a constant with dimensions of [strength] [length]$^{1/2}$ involving the element toughness, set by the material, and the flaw geometry and residual stress state, set by the manufacturing process. A typical value for $B = 1$ MPa m$^{1/2}$, such that a flaw size of $c = 25$ μm corresponds to a strength of $\sigma = 200$ MPa.[6] Setting

$$\sigma_{\mathrm{u}} = Bc_{\min}^{-1/2} \tag{5a}$$

gives the upper limit to the element strengths, σ_{u}, corresponding to the minimum in the population flaw-size distribution. Similarly,

$$\sigma_{\mathrm{th}} = Bc_{\max}^{-1/2} \tag{5b}$$

gives the lower limit to the element strengths, σ_{th}, corresponding to the maximum in the population flaw-size distribution. The lower bound to the strength, σ_{th}, is critical for design and is known as the "threshold strength."

The inverse relationship between strength and flaw size leads to some subtleties in relating population and sample quantities. The *complementary* cumulative distribution function, ccdf, $\bar{F}(c)$, for the element flaw population is related to the cdf by

$$\bar{F}(c) = 1 - F(c) \tag{6}$$

and is the tail distribution: the cdf $F(c)$ gives the probability that an element selected from the population has a flaw size smaller than c; the ccdf $\bar{F}(c)$ gives the probability that an element selected from the population has a flaw size $>c$. Just as the cdf $F(c)$ ranges between 0 and 1 over the domain $c_{\min} \leq c \leq c_{\max}$, the ccdf $\bar{F}(c)$ ranges between 1 and 0 over the same domain. $F(\sigma)$ and $\bar{F}(\sigma)$ may be similarly defined, where $F(\sigma)$ gives the probability that an element selected from the population has a strength $<\sigma$ and $\bar{F}(\sigma)$ gives the probability that an element has a strength $>\sigma$ and is commonly known as the "survivor function."[7] $F(\sigma)$ and $\bar{F}(\sigma)$ vary between 0 and 1 over the population conjugate strength domain $\sigma_{\mathrm{th}} \leq \sigma \leq \sigma_{\mathrm{u}}$. The inverse relationship between strength and flaw size leads to reversed

identification of the cdf and ccdf when c is substituted for σ using Equation (4) (large strengths imply small flaws and vice versa). In particular, Equation (6) becomes

$$F(c) = \bar{F}(\sigma) \tag{7}$$

enabling $F(c)$ to be determined if $\bar{F}(\sigma)$ is known, although it will be shown that explicit determination of $\bar{F}(\sigma)$ is not required in practice.

$\bar{F}(\sigma)$is the probability that a single fundamental element selected randomly from the population will have a strength $>\sigma$. If it is assumed that the elements (and thus their strengths) are independent, the probability $\bar{F}_{2\Delta A}(\sigma)$ that two elements selected from the population will both have strengths $>\sigma$ is given by the product of their probabilities taken singly[5]

$$\bar{F}_{2\Delta A}(\sigma) = \bar{F}(\sigma) \cdot \bar{F}(\sigma).$$

Thus, if k elements form a single component of area $A = k\Delta A$ and are independent, the probability, $\bar{F}_A(\sigma)$, that all k elements and thus the component have a strength $>\sigma$ is

$$\bar{F}_{k\Delta A}(\sigma) = \bar{F}_A(\sigma) = \bar{F}(\sigma)^k. \tag{8}$$

If a group of many similarly formed components, all of area A, is assembled, Figure 2, $\bar{F}_A(\sigma)$ is the proportion of components within the group that have a strength $>\sigma$. The fundamental elements in the population defined above contain single *strength-limiting* features or flaws (Figure 1) and thus k is the relative size of a component in terms of the number of strength-limiting features (eg, $k = 4$ in Figure 2). The number of strength-limiting features in a component will usually be much less than the number of *observable* features that are candidate flaws and k is thus expected to be a small number, much less than the number of observed pores, surface scratches, or edge chips.

The region of support and range of $\bar{F}_A(\sigma)$ are identical to those of $\bar{F}(\sigma)$. The cdf of a strength distribution is complementary to the ccdf, and thus the cdf for the group of component strengths, $F_A(\sigma)$, is given by

$$F_A(\sigma) = 1 - \bar{F}_A(\sigma) = \bar{F}(\sigma)^k \tag{9}$$

$F_A(\sigma)$ is the probability that a component of area A has a strength $<\sigma$, that is, the component will *fail* if exposed to a stress of σ. If a group of many similarly formed components is assembled, $F_A(\sigma)$ is the proportion of components within the group that will fail if exposed to a stress of σ and is thus the sought prediction. The sequence of prediction, from the specification of the fundamental population flaw pdf, $f(c)$, to the predicted sample strength cdf, $F_A(\sigma)$, is Equations 1,4,7,9. The following section describes factors required to implement reversal of this sequence from a measured strength distribution to the underlying flaw population.

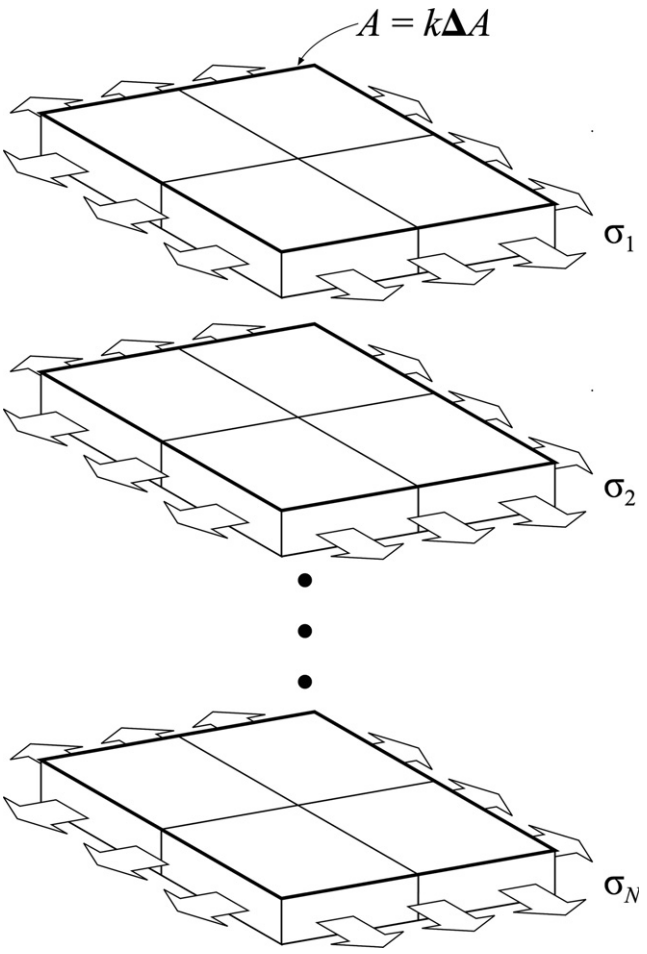

FIGURE 2 Schematic diagram of strength measurements of a group of identically sized components, surface area A (bold solid line) consisting of several fundamental elements ($k = 4$ shown)

2.2 | Flaw population determination

A first step in using the above framework to determine a flaw population is to recognize that an estimate of $F_A(\sigma)$ is required from the distribution of measured strengths. This is made clear by combining Equations (7) and (9) to gain

$$F(c) = [1 - F_A(\sigma)]^{1/k}, \tag{10}$$

which expresses the population flaw cdf in terms of the sample strength cdf. Equation (4) is implicit. As quantities from experimental measurements, σ and F_A can only exhibit discrete values. However, it is possible to estimate the continuous cdf of the population by a discrete function of the measured sample strengths. This function is termed the "empirical distribution function" (edf) and uses a simple ranking such that the function values are the fractions of observations within a sample that have strengths less than or equal to a specified strength. Operationally, for a sample containing N components, the component strengths are part of the sequence σ_i, in which the index i (or rank) runs from

1 to N. The sequence is ordered, such that σ_1 is the smallest measured strength and σ_N is the largest. The quantity $P_i = (i - 0.5)/N$ is formed for each strength; P_1 is the smallest number (near zero) and P_N is the largest (near 1). If a strength σ_i is selected from the ordered sequence, the conjugate P_i value gives the proportion of N for which the measured strengths are $<\sigma_i$: $P_i(\sigma_i)$ thus provides a statistical measure of $F_A(\sigma)$.

Direct substitution of $P_i(\sigma_i)$ for $F_A(\sigma)$ in Equation (10) provides a determination of discrete values of $F(c)$, provided additional experimental factors such as $\sigma(c)$ and k are known or assumed. Such discrete determinations have the advantage of representing as close to "raw data" as possible in flaw coordinates but have the extreme disadvantage of difficulty of interpretation as such determinations are one step removed from the fundamental material flaw pdf, $f(c)$, Equation (3). A much greater disadvantage of a discrete representation is that pointwise differentiation of $F(c)$ to obtain a discrete estimate of $f(c)$ leads to great scatter and variability.[2] Hence, a continuous "smoothing" function that describes discrete $P_i(\sigma_i)$ and that is amenable to smooth differentiation is required for substitution as $F_A(\sigma)$ in Equation (10).

As most ceramic flaw populations are unimodal, the conjugate strength cdf variations are sigmoidal, although the sigmoids may not be symmetric about the strength domain mid-point. A continuous smooth function with the flexibility to describe a range of sigmoidal strength cdf variations is

$$F(\mu) = \left(\frac{\mu^{3p}}{3} - \frac{\mu^{4p}}{2} + \frac{\mu^{5p}}{5}\right), \tag{11a}$$

where

$$\mu = \frac{\sigma - \sigma_{\mu\min}}{\sigma_{\mu\max} - \sigma_{\mu\min}} \tag{11b}$$

gives the relative strength position within the $F(\mu)$ domain. $\sigma_{\mu\min}$ and $\sigma_{\mu\max}$ are empirical fitting parameters, defining the minimum and maximum strength limits, respectively, of the smoothing domain and p is an empirical fitting parameter of order unity that controls the sigmoid symmetry. $\sigma_{\mu\min}$, $\sigma_{\mu\max}$, and p are sample-specific parameters and hence vary with test component size, geometry, and loading, distinguished from the invariant population characteristics σ_{th}, σ_u, and $F(\sigma)$. Key properties of $F(\mu)$ are $F(0) = 0$ and $F(1) = 1$ in accord with Equation (2) and $F'(0) = F'(1) = 0$. The shape of the sigmoid within the domain depends on p but the values and derivatives at the limits do not change: $p < 1$ skews the sigmoid to the left (more concave function), $p > 1$ skews the sigmoid to the right (more convex). Equation (11) can be best-fit to experimental σ data by selecting optimum bounding values of $\sigma_{\mu\min}$ and $\sigma_{\mu\max}$ to set the location and scale of the cdf and an optimum value of p to set the shape of the cdf. These steps and the differentiation to obtain $f(c)$ from Equation (3) are easily performed numerically, and this was the procedure here. The Appendix gives more details on Equation (11).

A near-to-final step, prior to such differentiation, in determining a flaw population is to express the best-fit continuum representation of measured sample strengths, Equation (11), in terms of flaw size, thereby connecting the right and left sides of Equation (10). In the framework development above, the Griffith relationship between strength σ and flaw size c was given, Equation (4), characterizing a simple surface crack shown in the schematic diagram of Figure 3A. This flaw type will be used below to interpret the strength measurements of the first set of ceramic materials.

As noted above, the flaw size or magnitude can also be dimensionless. Here, the dimensionless parameter χ is used to characterize the variable residual stress field amplitude locally surrounding a sharp indentation contact flaw. An indentation flaw, generated by contact load P, Figure 3B, consists of a residual contact impression contained within an approximately hemispherical, surface-localized plastic deformation zone (shown cross-hatched) that initiates and stabilizes cracks via the residual field.[8] The residual field and cracks determine the material strength adjacent to the flaw.[9] The stochastic nature of the contact impression and plastic zone formation lead to variability in the amplitude of the residual field and hence strength. This flaw type will be used to interpret the strength measurements of the second set of ceramic materials, as follows. The strength of an element containing a contact flaw generated by load P can be expressed by the ideal indentation-strength relation[9]

$$\sigma = \frac{Q}{(\chi P)^{1/3}} \tag{12a}$$

where Q is a constant with dimensions of [strength] [force]$^{1/3}$ involving the element toughness, set by the material, and the flaw geometry, set by the manufacturing process. The residual stress state of the flaw, characterized by χ, is also set by the manufacturing process and explicitly included in the strength expression. A typical value for $Q/\chi^{1/3} = 240$ MPa N$^{1/3}$, such that a flaw generated by a contact load of 8 N corresponds to a strength of $\sigma = 120$ MPa.[10] It is convenient to re-express Equation (12a) as

$$\sigma P^{1/3} = \frac{Q}{\chi^{1/3}} \tag{12b}$$

in which the indentation-strength quantity $\sigma P^{1/3}$ in Equation (12b) is contact load invariant and can be used directly in the estimation of the population of χ values. The similarity of Equations (4) and (12b) is clear and $\chi_{\min}$ and $\chi_{\max}$

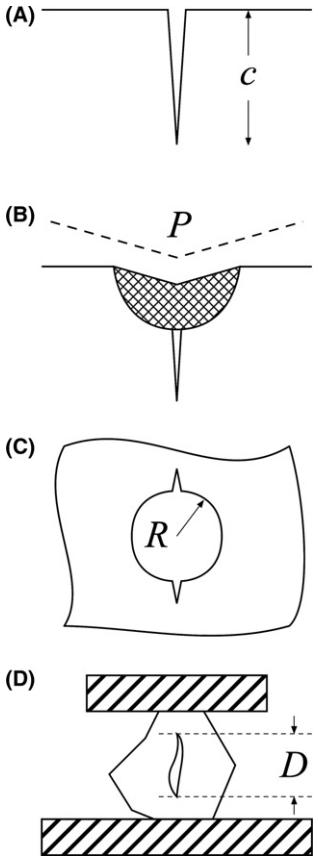

FIGURE 3 Schematic diagrams of strength-limiting flaws, applied tension is horizontal. A, Surface crack, length c. B, Surface indentation, peak load P. C, Bulk pore, radius R. D, Bulk void, characteristic size D

provide limits to the element strengths, including a threshold strength, similar to Equations 5(a) and (b). $f(\chi)$ and $F(\chi)$, characterizing the population of χ values at indentations, are analogous quantities to those involving c.

The first two flaw types were surface flaws, Figure 3A,B. The next two flaw types are bulk flaws. Near-spherical pores, radius R, with surrounding annular cracks were formed during sintering of a silicon nitride, the third materials set, Figure 3C. This flaw type will be used below to interpret silicon nitride strength measurements, obtained from published results.[11] The pore radius will be used to characterize the flaw size and the relation to strength is similar to Equation (4)[11,12]

$$\sigma = BR^{-1/2}, \tag{13}$$

where here B is a constant with dimensions of [strength] [length]$^{1/2}$ involving the element toughness, set by the material, and the flaw geometry, particularly the (annular crack size)/(pore radius) ratio, set by the manufacturing process. R_{min}, R_{max}, $f(R)$, and $F(R)$ characterize the population of R values and will be used in comparison with quantitative observations.[11]

Finally, irregularly shaped voids or delaminations, probably flattened ellipsoid-like with peripheral cracks, were formed in the bulk during heat treatment of refractory alumina grains, the fourth materials set, Figure 3D. This flaw type will be used to interpret strength measurements also obtained from published results.[13] Distinct from the first three sets of ceramics, which were tested in bending to generate tension on one surface, this material was tested in diametral compression between two platens, Figure 3D, leading to internal transverse tension. The refractory alumina grains consisted of single-crystal corundum particles loosely bound to leave internal voids of characteristic dimension D. The void dimension will be used to characterize the flaw size and the relation to strength is similar to Equations (4) and (13)

$$\sigma = BD^{-1/2}, \tag{14}$$

where here B is a constant with dimensions of [strength] [length]$^{1/2}$ involving the element toughness, set by the material, and the void geometry, set by the manufacturing process. D_{min}, D_{max}, $f(D)$, and $F(D)$ characterize the population of D values and will be used in comparison with qualitative observations.[13]

3 | EXPERIMENTAL METHODS

Nine ceramic systems were studied here, divided into four sets consisting of three, three, one, and two groups of components, respectively. The first set of three groups consisted of ceramic components with strengths controlled by flaws "intrinsic" to the component fabrication process: cordierite glass-ceramic discs containing surface scratches remnant from polishing; alumina bars containing side and edge chips and scratches remnant from sawing; and, silicon bars containing predominantly edge damage remnant from dicing. The second set of three groups consisted of ceramic components with strengths controlled by deliberately introduced indention flaws. Such flaws mimic contact damage generated by scratching and chipping in component fabrication and encountered by components at sharp contacts during operation.[14] This indented set included: bars of soda-lime silicate "window" glass; bars of a spodumene-based commercial glass-ceramic; and, discs of the cordierite mentioned above. Strength distributions for these first two groups of ceramics were determined by experimental measurements (see below). The third set consisted of one group of silicon nitride bend bars with strengths controlled by pores remnant from the sintering process.[11] The fourth set consisted of two groups of refractory ceramics: fused and tabular alumina grains with strengths controlled by internal voids and delaminations remnant from the thermal manufacturing process.[13] Strength distributions for these

last two groups of ceramics were determined by digitizing reported data.

For the first six ceramic systems, intrinsic and indented, strengths were measured under inert conditions in the absence of reactive species such as atmospheric moisture. For the discs, samples were mounted in a flat-on-three-ball biaxial flexure test fixture; the radius of the inner, upper flat was 2.5 mm and the radius of the outer, lower circle on which the specimens were supported by the three balls was 13.0 mm. For the bars, test specimens were mounted in a four-point uniaxial bending test fixture designed to minimize any torque on the specimens; the upper span varied from 3.0 to 15.0 mm and the lower span varied from 13.0 to 45.0 mm, depending on the size of the specimen. In both biaxial and uniaxial geometries, specimens were loaded to failure in 30 to 50 ms, minimizing any moisture effects on strength, and failure loads, F, recorded by a piezoelectric load cell. Disc specimens were examined to verify that failure had occurred in the uniform biaxial tensile stress region beneath the upper flat. Bar specimens were examined to verify that failure had occurred in the uniform uniaxial tensile stress region on the largest face beneath the upper span. In all cases, failure stresses, or strengths, σ were calculated from failure loads by $\sigma = \alpha F/d^2$, where d is the specimen thickness and α is a geometry term of order unity that depends on test fixture and specimen dimensions.[15]

The cordierite ($2MgO{\cdot}2Al_2O_3{\cdot}5SiO_2$) was a glass-ceramic material similar to that studied earlier[16] with a grain size of about 5 μm. The samples were in the form of discs, (29-32) mm diameter × (1.9-3.1) mm thick. The surface of the discs was polished to a reflective optical finish. In many cases of intrinsic strength measurement, a failure-inducing surface scratch was identifiable after testing. The alumina (Al_2O_3) was a commercial polycrystalline material (Coors AD995, Golden, CO) studied earlier,[17] consisting of 99.5% by weight Al_2O_3 with a grain size of approximately 5 μm. The material was in the form of bars 32 × 8 × 0.65 mm thick, sawn to size using a high-speed diamond saw and contained sawing damage on the long edges and small side faces. The large faces were sintered surfaces. In all cases of intrinsic strength measurement, failure originated at or near the edge of a bar, suggesting significant effect of sawing damage. The silicon (Si) samples were commercial single-crystal semiconductor devices diced to size along (110) from processed (001) wafers to produce two sets of bend bars (14.5 or 16.1) mm × (10.4 or 12.6) mm × 0.73 mm containing dicing damage along the long edges. The large faces were the processed faces and were placed in tension. Failure originated at or near the edge of a bar, suggesting significant effect of dicing damage; for some samples exhibiting small strengths, scratched surfaces were visible. One hundred and forty two cordierite intrinsic disc strengths, 100 Al_2O_3 intrinsic bar strengths, and 367 Si intrinsic die strengths were measured.

Prior to strength testing, the silicate glass, the commercial glass-ceramic, and selected cordierite specimens were indented in the center of a prospective tensile test face with a four-sided Vickers diamond pyramid. Indentation load P was varied from 1.96 to 294 N. The glass samples were taken from a commercial soda-lime silicate plate sawn into bend bars, 150 × 12 × 5.5 mm thick, and beveled along the long edge. The commercial glass-ceramic was a spodumene ($LiAlSi_2O_6$)-based material (Pyroceram C9606, Corning, New York) obtained as bars 105 × 6 × 5 mm thick with beveled edges, used previously.[18] The large surfaces of the bars were polished to the 1 μm diamond level to remove any surface stress from prior machining.[18] The cordierite samples were discs as above. All indented samples were examined after strength testing to verify that failure had originated at the indentation. One hundred and fourteen indented glass bar strengths, 67 indented spodumene bar strengths, and 149 indented cordierite disc strengths were measured.

The silicon nitride was a sintered material containing about 16% sintering aids by mass fraction and about 3% pores by volume fraction. An extensive pore size distribution study was completed on the as-fabricated sintered material,[11] revealing near-spherical pores with radii ranging from 1 to 35 μm and that >95% of pores were <5 μm in radius. Strength measurements were conducted using a three-point bend geometry with a span of 30 mm on bars 3 × 4 mm in cross section. Measurements on the fracture surfaces of the broken bend bars were performed to estimate the radii of the strength-controlling pores. The refractory alumina materials consisted of two groups of irregularly shaped grains representing the extremes of a larger extensive study.[13] Each group was sieved into a narrow size range: a group of "fused" alumina grains, 3.2 ± 0.1 mm in diameter, and a group of "tabular" alumina grains, 1.2 ± 0.1 mm in diameter. Both groups of grains consisted of aggregates of finer Al_2O_3 particles about 10 μm in diameter, with considerable porosity in the form of large, irregularly shaped voids between particles and fine spherical pores within particles. The fused material contained about 13% additives by mass fraction and was brown in color, the tabular material contained about 0.5% additives by mass fraction and was white. Strength measurements were conducted in compression between parallel platens and fracture surface observations were conducted. Twenty one silicon nitride bend strengths, 47 fused alumina crushing strengths, and 39 tabular alumina crushing strengths were digitized and analyzed.

4 | RESULTS

Figure 4 shows the measured edf strength responses, $P_i(\sigma_i)$, for the three sampled groups of ceramic materials containing intrinsic surface or edge flaws. The symbols represent individual strength measurements and all three responses are sigmoidal, if not fully symmetric. The solid lines represent visual best fits to the strength responses using the sigmoidal smoothing function polynomial of Equation (11) and directly adjusting the $\sigma_{\mu\min}$, $\sigma_{\mu\max}$, and p parameters (iterative numerical fitting was not required). The measured strengths were in the ranges typical of dense ceramics, 200-800 MPa, and the best fit functions described the measurements typically within ± 10 MPa over the ranges. Figure 5 shows the population flaw-size pdf curves, $f(c)$, deconvoluted from the three strength responses of Figure 4 using the above analysis. B values fix the domains of the deconvoluted flaw populations: $B = 1.4$ MPa $m^{1/2}$ (cordierite), $B = 2.5$ MPa $m^{1/2}$ (alumina), and $B = 0.75$ MPa $m^{1/2}$ (silicon) were used, reflecting the toughness values of the three materials. Within the fixed domains, k values set the shapes of the deconvoluted populations. As the exact values of k are unknown, a small value is used throughout, reflecting the likely very small density of strength-limiting flaws[2] and to enable simple comparisons. $k = 2$ was used for all three materials. k variations are discussed below but do not alter the conclusions.

The population crack length domains in Figure 5 are all a few tens of μm, typical of dense ceramics and reflecting the numerical values of the toughness and strengths above. However, the relative order of the crack length domains for the three materials is not the same as the strengths, reflecting the different B values (eg, silicon has mid-range strength, but the smallest flaw population). A clear feature of the populations in Figure 5 is that in all three cases $f(c)$ is asymmetric and significantly skewed to small flaw-sizes. The populations consist of a dominant number of small flaws and an extended tail of large flaws, a feature not clear from the nearly symmetric strength responses (and would be enhanced by increases in k). It also appears that all three deconvoluted populations have small-flaw nonzero minima, eg, about 10 μm in alumina, but there is no small-flaw information beyond the end of the curves, which reflect the strength-limiting flaws (not all flaws). A feature not apparent in Figure 5 is that all three deconvoluted populations have finite large-flaw maxima, about 65 μm, at which the extended tails vanish.

Figure 6 shows the measured strength responses, $\sigma(P)$, for the three sampled groups of ceramic materials containing indentation flaws. The symbols represent individual strength measurements at the indentation loads indicated and the solid lines represent best fit ideal indentation-strength parameters, Equation (12b), of $Q/\chi_{ave}^{1/3} = 140$ MPa $N^{1/3}$ (soda-lime glass), 450 MPa $N^{1/3}$ (spodumene), and 240 MPa $N^{1/3}$ (cordierite), where χ_{ave} are average values of the residual stress amplitude acting over the indentation loads used. Although the best fit lines clearly describe the observations over nearly two orders of magnitude of indentation load, there are some deviations. Significantly, at large loads the strength data ranges do not include the ideal responses, reflecting variable reductions in the indentation stress fields from disrupting lateral cracks and chipping. These effects are most pronounced in soda-lime glass and less so in cordierite, Figure 6A,C, respectively. Figure 7 shows the measured edf indentation-strength responses, $P_i(\sigma P^{1/3})$, for the three groups of indented materials using the data of Figure 6. The symbols represent

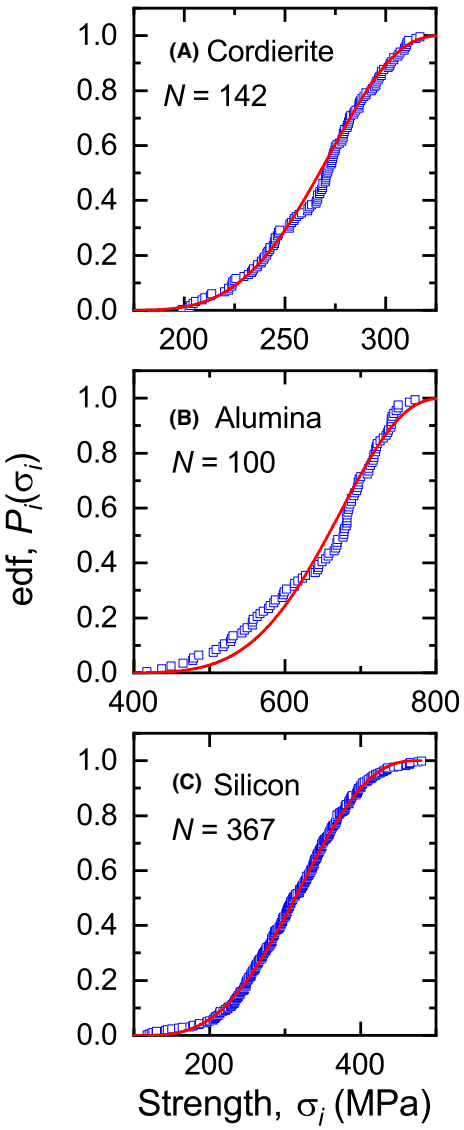

FIGURE 4 Plots of measured strength edf (symbols) and cdf best fits (lines) for (A) cordierite glass-ceramic (surface flaws), (B) polycrystalline alumina (edge flaws), and (C) single crystal silicon (edge flaws) [Color figure can be viewed at wileyonlinelibrary.com]

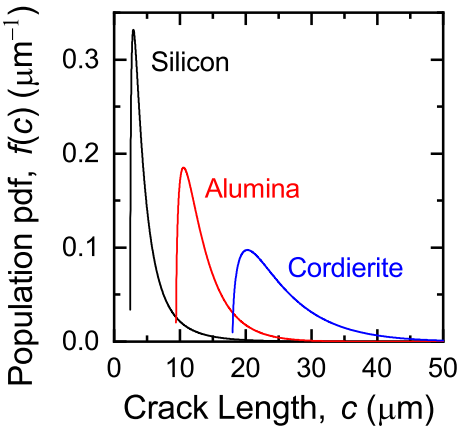

FIGURE 5 Plots of deconvoluted flaw populations for the three materials in Figure 4 [Color figure can be viewed at wileyonlinelibrary.com]

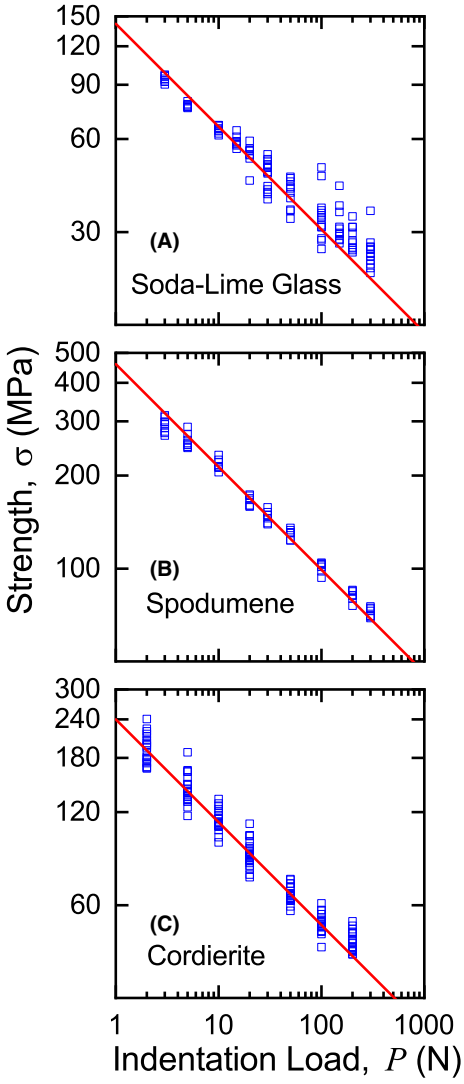

FIGURE 6 Plots of strength vs indentation load for three ceramic materials. Solid lines indicate ideal indentation-strength behavior. A, SL glass. B, Spodumene. C, Cordierite [Color figure can be viewed at wileyonlinelibrary.com]

individual indentation-strength measurements and all three responses are sigmoidal but not symmetric. The solid lines represent visual best fits to the responses using the sigmoidal smoothing function polynomial of Equation (11); in two cases, Figure 7A,C, the measured responses were markedly concave and at small values the responses were not fully described by the fits.

Figure 8 shows the population residual stress amplitude pdf curves, $f(\chi)$, as functions of χ/χ_{ave}. These curves were deconvoluted from the three indentation-strength edf responses of Figure 7 using the above analysis and the best-fit $Q/\chi_{ave}^{1/3}$ values from Figure 6. The indentations were the known dominant single flaw in the test specimens represented in the strength measurements of Figures 6 and 7 and hence the ensemble of test specimens constituted the population of elements. Thus, $k = 1$ represents the edf measurements in Figure 7 and was used to generate Figure 8. The pdf curves in Figure 8 differ from those in Figure 5 as they represent relative population dispersions about the mean value, $\chi/\chi_{ave} = 1$, of the indentation residual field. The spodumene response is narrow and close to symmetric with convex wings surrounding a concave center (bell shaped), reflecting small scatter of the strength measurements about an ideal response in Figure 6. The implication is that the amplitudes of the indentation residual fields represented in Figure 6B were nearly constant. The soda-lime glass and cordierite responses are broad and also symmetric but exhibit almost complete concave behavior, reflecting increased scatter and systematic deviation from ideal responses in Figure 6; the deviation is also visible in the abrupt changes in derivative. The implication here is that the indentation residual fields represented in Figure 6A,C exhibited significant systematic reductions. An interpretation of Figure 8 is that increased lateral cracking and chipping perturbed a spodumene-like response to be more glass- and cordierite-like through introduction of smaller χ values.

Figure 9A shows the measured edf strength response, $P_i(\sigma)$, for the silicon nitride material. The symbols represent individual strength measurements[11] and the response is sigmoidal. The solid line represents a visual best fit to the response using the sigmoidal smoothing function polynomial of Equation (11). Figure 9B shows two measured cdf pore size responses, $F(R)$, for the material. The dashed line in Figure 9B represents the observations of over 4000 pores in the as-fabricated material.[11] The distribution is clearly dominated by very many small pores with $R < 5$ μm and a few large pores with $R \approx 20$ μm. The symbols in Figure 9B represent the observations of pores identified as failure sites on fracture surfaces from strength tests. This distribution represents only pores with $R \approx 20$ μm. The bold solid line and

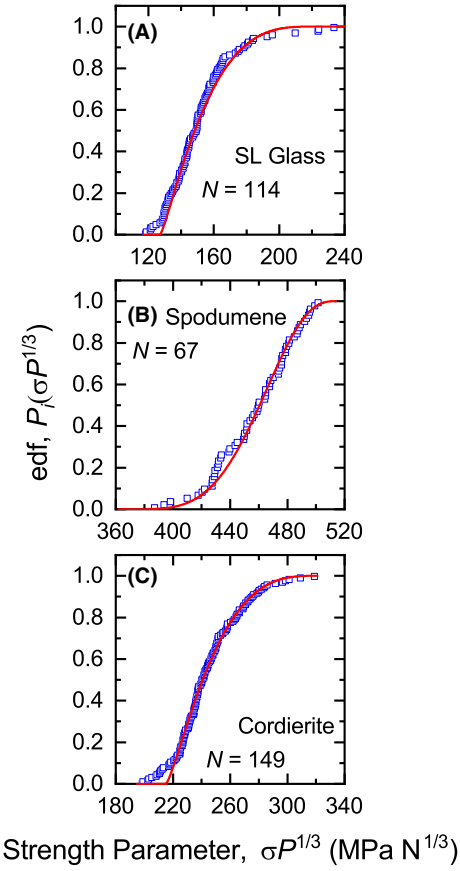

FIGURE 7 Plots of measured residual stress edf (symbols) and cdf best fits (lines) for the three materials in Figure 6. A, SL glass. B, Spodumene. C, Cordierite [Color figure can be viewed at wileyonlinelibrary.com]

shaded region in Figure 9B represent the deconvolution of the strength data in Figure 9A using the above analysis and bounds of $B = (4.15 \pm 0.25)$ MPa m$^{1/2}$ and $k = 1.7 \pm 0.3$. The bounds of B are comparable to the toughness of silicon nitride, about 4.5 MPa m$^{1/2}$, consistent with the fracture mechanics of pores.[12] The bounds of k, as noted by Chao and Shetty,[11] are much, much less than the expectations from observations of pore density in the as-fabricated material. The implication is that very few of the observed pores constitute strength-controlling flaws. Chao and Shetty suggest that large aspect ratios and associated, but un-observed, cracks distinguish strength-controlling flaws from the much greater number of pores. A similar conclusion was reached regarding surface roughness on MEMS devices, in which very few of the observed surface crevices were regarded as strength-controlling flaws.[2] Figure 9C shows the associated pore size pdf curves from Figure 9B using the same distinguishing notation for as-fabricated and failure inducing pores. As suggested, the as-fabricated pore size population is dominated by small, sub-5 μm pores with an extended tail out to 35 μm. The limits of the strength-limiting pores at failure are skewed distributions extending from about 15 to 35 μm. The

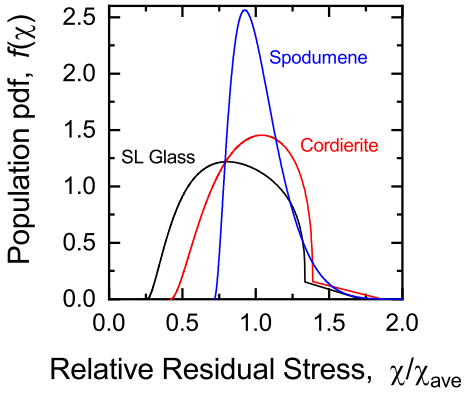

FIGURE 8 Plots of deconvoluted residual stress populations for the three indented materials in Figures 6 and 7 [Color figure can be viewed at wileyonlinelibrary.com]

implication once again is that only very few of the largest observed features are flaws.

Figure 10A shows the measured edf strength responses, $P_i(\sigma)$, for the two refractory alumina materials. The symbols represent individual strength measurements[13] and the responses are sigmoidal. The solid lines represent visual best fits to the responses using the sigmoidal smoothing function polynomial of Equation (11). The extremes of the measurements are shown, in which larger fused alumina grains are weaker than smaller tabular alumina grains. Figure 10B shows the population flaw-size pdf curves, $f(D)$, deconvoluted from the two strength responses of Figure 10A using the above analysis. The B values were fixed by Equation (14) such that the smallest strength observed for each material, about 2 MPa and 17 MPa for fused and tabular, respectively, led to strength-limiting void sizes no larger than the grain sizes, about 3 and 1 mm, respectively. The consequent values were $B = 0.11$ MPa m$^{1/2}$ (fused alumina) and $B = 0.58$ MPa m$^{1/2}$ (tabular alumina). $k = 2$ was used. The void size populations in Figure 10B are extremely similar; dominated by voids about 10 μm in size with greatly extended tails at larger void sizes. The deconvoluted void sizes are comparable to the observed interparticle fissures[13] but much larger than the intraparticle pores, consistent with the small B values reflecting weak interparticle bonding. Consistent with the insights of Bertrand et al,[13] the fused material is weaker (less strong, less tough) than the tabular material, but contrary to the views of Bertrand et al, as the toughness of corundum (or sapphire) is ≈ 3 MPa m$^{1/2}$, it does not appear that the grain fracture behavior is related to the fracture of sapphire.

5 | DISCUSSION AND CONCLUSIONS

The analysis here has been applied successfully in determination of underlying flaw populations from measured

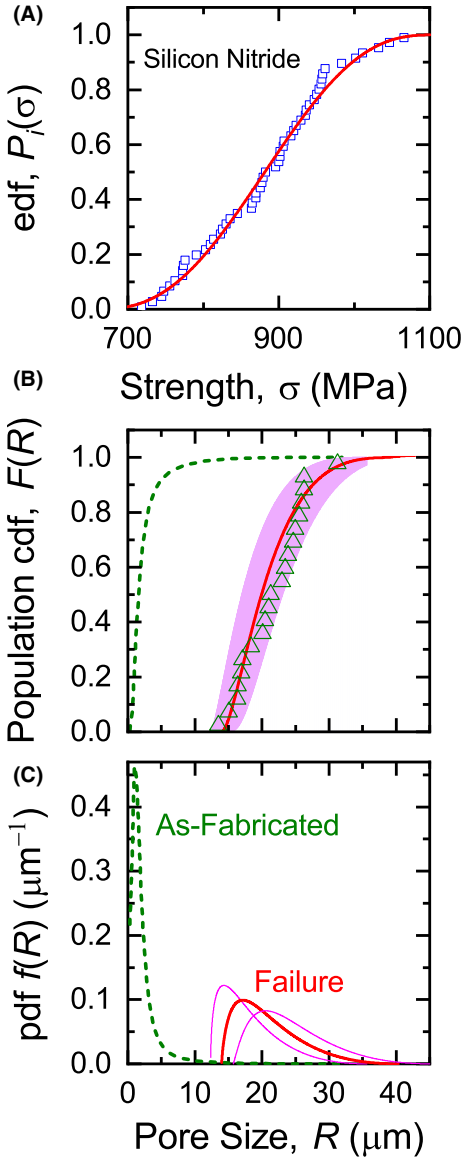

FIGURE 9 A, Plot of measured strength edf (symbols) and cdf best fit (line) for silicon nitride. Measurements from Chao and Shetty.[11] B, Plot of measured pore size cdf for as-fabricated (dashed line) and strength tested (symbols) silicon nitride. Shaded region indicates bounds on deconvolution from strength measurements. C, Plot of measured pore size pdf for as-fabricated (dashed line) and strength-tested (solid lines) silicon nitride [Color figure can be viewed at wileyonlinelibrary.com]

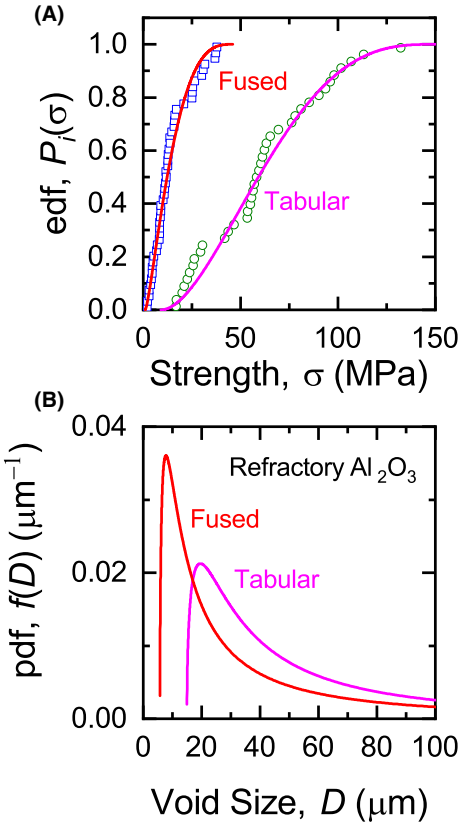

FIGURE 10 A, Plot of measured strengths edf (symbols) and cdf best fits (lines) for refractory alumina grains. Measurements from Bertrand et al[13] B, Plot of deconvoluted void size pdf curves [Color figure can be viewed at wileyonlinelibrary.com]

sample strength distributions on a wide variety of ceramic systems. Nine systems—encompassing seven materials, including glass, glass-ceramics, single crystal, and polycrystals—and four flaw types, including bulk, surface, and edge—attest to the wide applicability of the methods developed. In many cases, aspects of the flaw populations deconvoluted from the strength measurements are in agreement with independent observations, further supporting the methods. The broadest implication from this work is that strength distribution measurements are a rich source of useful quantitative information for the ceramic manufacturer and designer rather than qualitative comparative information. Numerical specification of a flaw population enables quantitative decisions regarding manufacturing yield, reliability prediction, and design outcomes, well beyond the qualitative inference that "large strengths mean small flaws."

The narrower implications of the work apply to specific ceramic systems. For example, it is clear from Figure 5 that the population of dicing flaws in silicon is smaller than the population of sawing flaws in alumina, and that both are smaller than the polishing flaws in cordierite. As silicon is less tough than alumina, this observation needs to be true so that the material strengths and thus the load bearing capacities of comparably sized components are also comparable—considerations that are important in attaching silicon dies to alumina substrates in microelectronics manufacturing. Figure 5 enables manufacturing-related questions such as "Is the disparity in flaw sizes due to the alumina microstructure or the silicon dicing procedure?" and "How can sawing be more benign than polishing?" to be addressed. Figure 8 makes clear that although indentations

are "controlled" flaws, that populations of indentation flaws are not all identical in residual stress characteristics. From a materials-testing point of view,[10] this is acceptable providing the residual stress is not too small.[9] Figure 8 enables an assessment of the proportion of the test population that are unacceptable. Figure 10 makes clear that the flaw sizes in fused and tabular refractory alumina are comparable and that differences between the two materials reflect different internal interface characteristics rather than differences of the constituent crystals.

Figure 9, however, probably has the greatest implication for interpretations of strength distribution measurements. Figure 9 includes a direct comparison of the sizes of pores causing failure with those from the entire as-fabricated population. It is clear that the pores causing failure are a very small fraction of the population, reinforcing that, used alone, observations of populations of suspected strength-limiting flaws can be extremely misleading with regard to strength expectations. The analysis here makes clear that strength measurements can be used to determine flaw populations, exemplified by the experimental agreements in Figure 9—they are, of course, by definition, the *strength-limiting* flaw populations. This distinction is supported by previous strength measurements on small-scale silicon structures, for which roughness observations can greatly over-estimate the number of strength-limiting surface flaws.[2] If the domain of observations is restricted to strengths, a further, numerical, implication also supported by the previous observations,[2] is that the values of k are small. The elemental volumes, areas, or lengths containing single flaws are comparable to typical strength test specimen dimensions.

Detailed consideration of the work of Chao and Shetty,[11] summarized in Figure 9, further supports this point. Chao and Shetty showed that the distribution of largest pores observed in samples of pores from the observed population was consistent with an extreme value formulation. The same formulation was used to fit the number of pores existing in strength tested samples, based on the observed population and the distribution of measured strength-limiting pore sizes. Values of k for the strength tested samples of 500-2000 were fit and shown to be consistent with the measured strength distribution based on a fracture mechanics methodology. The points above regarding strength-limiting flaw populations were based on the observation that these fitted values were much less than the predicted test specimen size of approximately 10^5. The disparity between the earlier $k \approx 10^3$ value and the small $k \approx 2$ value used here is that the analysis of Chao and Shetty assumed that the observed pore population was the strength-controlling flaw population. In fact, this is in stark contrast to the point here that a small proportion of the observed pore population acts as the strength-limiting flaws. The ratio of fitted to predicted specimen size suggests that only about 1% of the observed pores contributed to the strength-controlling population, corresponding to a lower bound size for the strength-controlling flaw population of about 13 μm, consistent with Figure 9. Using this bound and the information in Chao and Shetty gives a fitted k range of about 3.5-14, much closer to the value inferred here. Full agreement probably requires greater experimental knowledge of the relation between strength and pore size: Chao and Shetty enforced agreement between the observed pore population and the failure inducing pore distribution to predict the strength distribution. Here, agreement was enforced between the strength distribution and the failure inducing pore distribution to infer a strength controlling pore population.

Finally, there are two principal methods of verifying the methodology demonstrated here for future work. The first, discussed above, is to compare flaw populations inferred from strength measurements with direct observation. The second is to compare strength distributions determined on components of different sizes containing flaws drawn from the same population. This method is limited, in that only the ratio of the k values for the components is obtainable but engineered test geometries that constrain k to small values (even 1) such as notches and single particles, in addition to known size ratios, provide additional information. Experiments to evaluate exact values of k, and therefore enable greater confidence in manufactured component performance prediction from sampled strength measurements, must be seen as a priority in this field.

ACKNOWLEDGMENTS

Certain commercial equipment, instruments, or materials are identified in this paper in order to specify the experimental procedure adequately. Such identification is not intended to imply recommendation or endorsement by the National Institute of Standards and Technology, nor is it intended to imply that the materials or equipment identified are necessarily the best available for the purpose.

ORCID

Robert F. Cook https://orcid.org/0000-0003-0422-8881
Frank W. DelRio https://orcid.org/0000-0003-1727-8220

REFERENCES

1. Ashby MF. *Materials selection in mechanical design*. Oxford, UK: Butterworth-Heinemann; 1999.
2. Cook RF, DelRio FW. Material flaw populations and component strength distributions in the context of the Weibull

function. Exp Mech. 2018. https://doi.org/doi:10.1007/s11340-018-0423-2
3. DelRio FW, Cook RF, Boyce BL. Fracture strength of micro- and nano-scale silicon components. Appl Phys Rev. 2015;2:021303-1-51.
4. Cook RF. Long-term ceramic reliability analysis including the crack-velocity threshold and the "bathtub" curve. J Am Ceram Soc. 2018;101:5732–44.
5. Walpole RE, Myers RH. *Probability and statistics for engineers and scientists*. New York, NY: Macmillan Publishing Co., Inc; 1972.
6. Lawn BR. *Fracture of brittle solids*, 2nd edn. Cambridge, UK: Cambridge University Press; 1993.
7. Castillo E. *Extreme value theory in engineering*. New York, NY: Academic Press, Inc; 1988.
8. Lawn BR, Evans AG, Marshall DB. Elastic/plastic indentation damage in ceramics: the median/radial crack system. J Am Ceram Soc. 1980;63:574–81.
9. Marshall DB, Lawn BR, Chantikul P. Residual stress effects in sharp contact cracking Part 2 Strength degradation. J Mater Sci. 1979;14:2225–35.
10. Cook RF. Multi-scale effects in the strength of ceramics. J Am Ceram Soc. 2015;98:2933–47.
11. Chao L-Y, Shetty DK. Extreme-value statistics analysis of fracture strengths of a sintered silicon nitride failing from pores. J Am Ceram Soc. 1992;75:2116–24.
12. Shetty DK, Rosenfield AR, Duckworth WH. Biaxial stress state effects on strengths of ceramics failing from pores. In: Bradt RC, Evans AG, Hasselmann DPH, Lange FF, editors. *Fracture mechanics of ceramics volume 5 surface flaws, statistics, and microcracking*. New York, NY: Plenum Press, 1983; p. 531–42.
13. Bertrand PT, Laurich-McIntyre SE, Bradt RC. Strengths of fused and tabular alumina refractory grains. Am Ceram Soc Bull. 1988;67:1217–22.
14. Lawn BR, Hockey BJ, Richter H. Indentation analysis: application in the strength and wear of brittle materials. J Microsc. 1983;130:295–308.
15. Roark RJ, Young WC. *Formulas for stress and strain*, 5th edn. Tokyo, Japan: McGraw-Hill; 1983.
16. Cook RF. Toughening of a cordierite glass-ceramic by compressive surface layers. J Am Ceram Soc. 2005;88:2798–808.
17. Cook RF. Fracture mechanics of the scratch strength of polycrystalline alumina. J Am Ceram Soc. 2017;100:1146–60.
18. Cook RF, Lawn BR, Dabbs TP, Chantikul P. Effect of machining damage on the strength of a glass-ceramic. J Am Ceram Soc. 1981;64:C121–2.
19. Abramowitz M, Stegun I (eds). *Handbook of mathematical functions*. Washington, DC: US Government Printing Office; 1964.
20. Johnson NL, Kotz S. *Continuous univariate distributions - 2*. Boston, MA: Houghton Mifflin Company; 1970.
21. Kotz S, van Dorp JR. *Beyond beta*. Hackensack, NJ: World Scientific; 2004.

How to cite this article: Cook RF, DelRio FW. Determination of ceramic flaw populations from component strengths. *J Am Ceram Soc*. 2019;102:4794–4808. https://doi.org/10.1111/jace.16262

APPENDIX A1

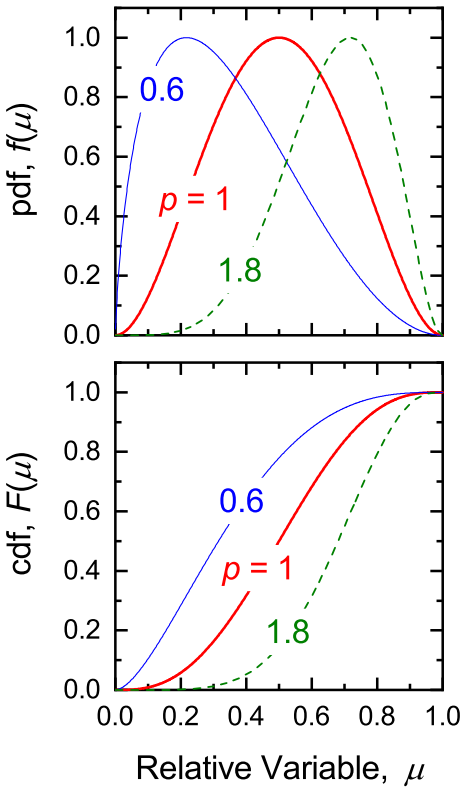

FIGURE A1 Plots illustrating behavior of the bounded polynomial distribution function used to fit strength edf measurements. A, pdf curves for various values of shape parameter p. B, Conjugate cdf curves. [Color figure can be viewed at wileyonlinelibrary.com]

BOUNDED POLYNOMIAL PROBABILITY DISTRIBUTIONS

It is convenient to use simple expressions for the continuous pdf and related cdf such that: (a) relations between the pdf and cdf are easily expressed; (b) the discrete edf derived from a sample of a population is easily fit by a continuous cdf expression; (c) the relations between population and sample functions are easily expressed; and, (d) (probably most important) the expressions describing the pdf and cdf contain parameters that represent physical quantities. In consideration of samples of strengths, key physical quantities are the upper and lower bounds, σ_u and σ_{th}, respectively, with reversed bounds of the conjugate flaw size, c_{min} and c_{max}.

A simple polynomial pdf expression $f(x)$, where x is a general random variable, that meets the requirements above is

$$f(x) = A(x - x_{min})^u (x_{max} - x)^v, \quad \text{(A1)}$$

where x_{max} and x_{min} are upper and lower bounds on the pdf such that $f(x<x_{min}) = f(x>x_{max}) = 0$, u and v are

exponents characterizing the shape of the pdf within the bounds, and A is a normalizing parameter. It is convenient to re-express Equation (A1) using a dimensionless scaled variable μ, with

$$\mu = \frac{x - x_{\min}}{x_{\max} - x_{\min}} \tag{A2}$$

such that

$$f(\mu) = A(x_{\max} - x_{\min})^{u+v}\mu^u(1-\mu)^v,$$

making clear that Equation (A1) is functionally equivalent to the beta distribution, differing only in notation and normalization.[19,20] A minimal specific expression has $u = v = 2$, such that Equation (A2) becomes

$$f(\mu) = A(x_{\max} - x_{\min})^4(\mu - \mu^2)^2, \tag{A3}$$

which describes a symmetric unimodal pdf with values and derivatives that smoothly vanish at the bounds; $f(0) = f(1) = f'(0) = f'(1) = 0$, a "bell-shaped" curve, Figure A1(A), that represents many physical pdfs.

As in Equation (1), the cdf $F(x)$ is related to the pdf by integration

$$F(x) = \int_0^x f(x')\mathrm{d}x'. \tag{A4}$$

Recognizing that

$$\frac{\mathrm{d}\mu}{\mathrm{d}x} = \frac{1}{(x_{\max} - x_{\min})},$$

Equation (A4) becomes, on using Equation (A3),

$$F(\mu) = A(x_{\max} - x_{\min})^5 \int_0^\mu (\mu'^2 - 2\mu'^3 + \mu'^4)\mathrm{d}\mu'$$

and thus

$$F(\mu) = A(x_{\max} - x_{\min})^5\left(\frac{\mu^3}{3} - \frac{\mu^4}{2} + \frac{\mu^5}{5}\right), \tag{A5}$$

and is a specific algebraic instance of the incomplete beta function.[19,20] Normalization requires $F(1) = 1$, such that $A = 30/(x_{\max} - x_{\min})^5$ and thus, Equation (A5) becomes

$$F(\mu) = 30\left(\frac{\mu^3}{3} - \frac{\mu^4}{2} + \frac{\mu^5}{5}\right) \tag{A6}$$

and thus, from Equation (A4),

$$f(\mu) = \frac{30}{(x_{\max} - x_{\min})}(\mu - \mu^2)^2. \tag{A7}$$

Equation (A6) describes a function that is antisymmetric about (1/2, 1/2) with values $F(0) = 0$ and $F(1) = 1$ and derivatives that smoothly vanish at the bounds with $F'(0) = F'(1) = 0$, a sigmoidal curve, Figure A1(B), that represents many physical cdfs.

The applicability of Equation (A6) can be expanded to asymmetric distributions by generalizing the argument through the transformation $\mu \mapsto \mu^p$ where $p > 0$ is an empirical exponent of order unity, such that

$$F(\mu) = 30\left(\frac{\mu^{3p}}{3} - \frac{\mu^{4p}}{2} + \frac{\mu^{5p}}{5}\right). \tag{A8}$$

The shape of the sigmoid within the bounds now depends on p but the values and derivatives at the bounds do not change. Examples are shown in Figure A1(A,B). Equation (A8) can be best fit to experimental x data by selecting optimum bounding values of $x_{\min}$ and $x_{\max}$ to set the location and scale of the cdf and an optimum value of p to set the shape of the cdf: these steps are best performed numerically as is the transformation to obtain $f(\mu) = \mathrm{d}F(\mu)/\mathrm{d}\mu$.

The well-known Weibull cdf, W, written using the same notation, is[5]

$$W(\mu) = 1 - \exp(-\mu^m). \tag{A9}$$

There are clear similarities between Equations (A8) and (A9): the forms are set (polynomial and stretched exponential) and both generate sigmoidal responses $0 \le F,\ W \le 1$ over the domain $0 \le \mu$; the location and scale are both set by the Equation (A2) relating x and μ, resulting in lower bound $0 \le \mu$; and, the shape is set by a single parameter (p and m). The differences between the two expressions lie in the existence of the upper bound and the interpretation of the lower bound. The polynomial is upper-bounded by $\mu \le 1$ and $F(1) = 1$. The Weibull function is unbounded for large μ: $x_{\max}$ is simply a location and scale parameter, $\mu > 1$ is possible and only asymptotically does $W(\mu) \to 1$ for $\mu \gg 1$. The lack of an upper bound in the Weibull function does not usually present difficulties in a mathematical sense as $x_{\max}$ can simply be treated as a fitting parameter to describe the dispersion of x. However, if x is *physically* related to an underlying quantity y by the transformation $x \mapsto y^{-w}$, $(w > 0)$ the infinite upper bound to x implies a zero lower bound for y, which may not be physical. In particular, of relevance here, is the usual inverse quadratic relationship between strength and flaw size, $\sigma \sim c^{-1/2}$, such that if W is fit to strength data, the resulting flaw size cdf and pdf expressions include minima of zero. As the smallest flaws in a population do not usually affect mechanical performance and their lack of existence is difficult to disprove this is not an issue. Of more concern is that in many cases $x_{\min} = 0$ is selected such that $x_{\max}$ is reduced to a scale parameter. Although the mathematical definition of μ is unaffected, in the x, y formalism above

the zero lower bound to x implies an infinite upper bound for y that is not physical. In strength-flaw size considerations, setting a zero lower bound to strength implies an infinite upper bound to flaw size. Empirically, non-zero lower bounds to strength are *always* observed, consistent with the fact that all manufacturing processes must use a finite amount of energy and therefore must generate a finite upper bound flaw size. Hence, on physical grounds, the bounded polynomial expression is preferred to the Weibull expression, although it is not unique. Other bounded pdf forms giving rise to flexible sigmoidal cdf expressions (eg, the triangle distribution[21]) have the same advantages. Unbounded pdf forms that give rise to flexible cdf sigmoids (eg, the Gamma distribution[5,20]) have the disadvantages of requiring additional parameters to characterize shape or truncation and although capable of describing experimental data may not be as easily manipulated analytically as the polynomial expression.